The Journal of The Textile Institute

ISSN: 0040-5000 (Print) 1754-2340 (Online) Journal homepage: https://www.tandfonline.com/loi/tjti20

A comparative computational study of blood flow pattern in exemplary textile vascular grafts

Raúl A. Valencia, Manuel J. García & John Bustamante

To cite this article: Raúl A. Valencia, Manuel J. García & John Bustamante (2018) A comparative computational study of blood flow pattern in exemplary textile vascular grafts, The Journal of The Textile Institute, 109:7, 858-870, DOI: 10.1080/00405000.2017.1380872

To link to this article: https://doi.org/10.1080/00405000.2017.1380872

THE JOURNAL OF THE TEXTILE INSTITUTE, 2018
VOL. 109, NO. 7, 858–870
https://doi.org/10.1080/00405000.2017.1380872

A comparative computational study of blood flow pattern in exemplary textile vascular grafts

Raúl A. Valencia[a], Manuel J. García[b] and John Bustamante[c]

[a]Department of Textile and Mechanical Engineering, Universidad Pontificia Bolivariana and Universidad EAFIT, Medellín, Colombia; [b]Department of Mechanical Engineering, The University of Texas, San Antonio, TX, USA; [c]Cardiovascular Dynamics Research Group, Universidad Pontificia Bolivariana, Medellín, Colombia

ABSTRACT

Textile vascular grafts are biomedical devices and play an important role serving as a solution for the partial replacement of damaged arterial vessels. It is believed that the success of a textile vascular graft, in the healing process after implantation, is due to the porous micro-structure of the wall. Although the transport of fluids through textiles is of great technical interest in biomedical applications, little is known about predicting the micro-flow pattern and cellular transport through the wall. The aim of this work is to investigate how the type of fabric, permeability and porosity affect both the local fluid dynamics at several scales and the fluid-particle interaction between platelets in textile grafts, related with the graft occlusion. This study involves both experimental and computational tests. Experimental tests are performed to characterize the permeability and porosity according to the ISO 7198 standard. The numerical process is based on a multi-scale approach where the fluid flow is solved with the Finite Element Method and the discrete particles are solved with the Molecular Dynamic Method. The results have shown that the type of fabric in textile vascular grafts and the degree of porosity and permeability affect both the local fluid dynamics and the level of penetration of platelets through the wall, thus indicating their importance as design parameters.

ARTICLE HISTORY
Received 8 September 2015
Accepted 11 September 2017

KEYWORDS
Textile vascular grafts; porous media; local fluid dynamics; fluid-particle interactions; multi-scale approach

Introduction

Atherosclerosis accounts for almost one half of all deaths in Europe (Chlupac, Filova, & Bacakova, 2009) and each year, 1.4 million patients in the U.S.A. need vascular prostheses (Hasan et al., 2014). Vascular grafts play an important role like biomedical devices serving as a solution for the partial replacement of damaged arterial vessels, to prevent rupture from aneurysms, to overcome obstructions in the aorta or other major arteries, as well as for vascular access (renal dialysis) (Tura, 2003).

Straight and bifurcated fabric grafts are available in a wide variety of sizes and shapes, ranging from 4 to 35 mm in diameter (Tura, 2003). The options which are currently available for these transplants are biological grafts and synthetic grafts with biomedical textiles. Biological grafts are the preferred materials to reconstruct vascular segments, but their use is limited due to the lack of tissue donors, patients with previous interventions or anatomical variability. For that reason, synthetic grafts are widely used (Bergmeister, Strobl, Grasl, Liska, & Schima, 2013). The most commonly used materials in synthetic grafts are Polytetrafluoroethylene or PTFE (Teflon), Polyethylene Terephthalate or PET (Dacron), ePTFE (expanded form of Teflon) and synthetic polymers (Bronzino, 2000). The different techniques used to manufacture textile grafts have an effect on the final device properties and on the site for grafting (Kutz, 2003). For instance, woven dacron grafts are one of the major choices available for prosthetic reconstruction in large diameters and are predominantly used in the repair of ruptured abdominal aortic aneurysms. In recent years, the interest in another technique called electrospinning has increased exponentially to create new vascular grafts in small diameters (Hasan et al., 2014). These fabrics with nano/microscale fibers and a large surface area have a great potential for mimicking the microenvironment of blood vessels. However, their application on humans has not yet been achieved.

It is believed that the success of a textile vascular graft is due to the porous micro-structure of the wall (Vafai, 2011). Some geometric characteristics to define the porous wall are the type of fabric, the degrees of porosity and permeability, thickness, pore size and the specific surface area, among others (Pham, Sharma, & Mikos, 2006). For instance, porosity allows different levels of penetration of the cells and the irrigation of fluid with nutrients through the graft wall, providing a scaffold for tissue repair process (Berthier & Silberzan, 2010). The permeability prevents bleeding. Both properties are key factors for normal hemostasis after implantation (Tura, 2003). In that biological process, the local fluid dynamics and the cellular transport may be affected by the type of textile vascular graft, exerting different reaction forces on cells (Vafai, 2011). Although the transport of fluids through textiles is of great technical interest in biomedical applications, little is known about predicting the micro-flow pattern and cellular transport through the wall. Many aspects of flow through a fabric can only be understood on a microscopic level (Leisen, Beckham, & Farber, 2004), but this information is difficult to obtain experimentally both *in vivo* and in vitro, representing a great deal of research efforts (Cioffi, Boschetti, Raimondi, & Dubini, 2006). For instance,

CONTACT Raúl A. Valencia raul.valencia@upb.edu.co, rvalenc2@eafit.edu.co

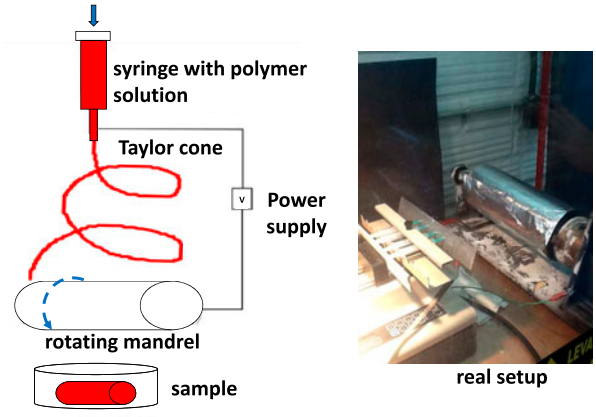

Figure 1. Electrospinning setup: schematic representation of a electrospinning machine (left) and picture of the real setup (right).

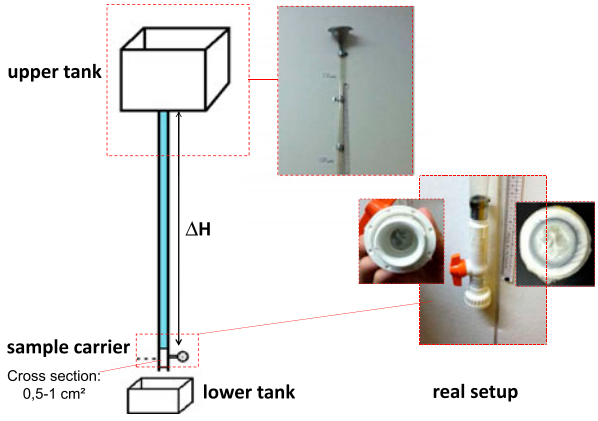

Figure 2. Permeability setup: schematic representation of a vertical column of water (left) and image of the real setup (right).

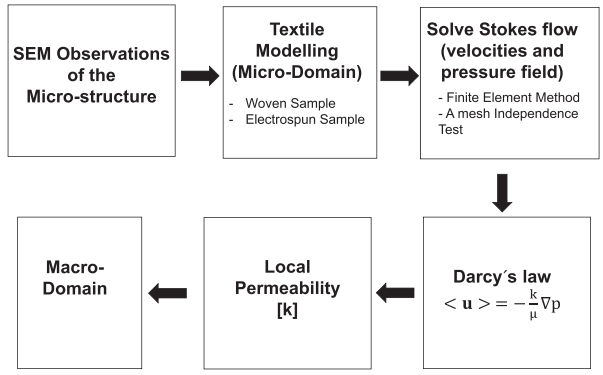

Figure 3. Flowchart to compute the permeability via computational methods.

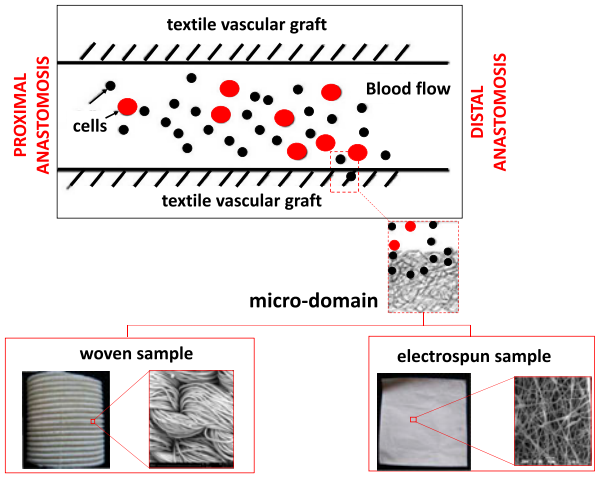

Figure 4. Textile graft at micro-scale. Unit cell with two possible configurations: woven and electrospun.

Laser Doppler Velocimetry or Particle Image Velocimetry (PIV) can only measure the local velocities outer walls, but this is not relevant to quantify the influence of the type of fabric and the shear stress on cells inside the live graft wall. Additionally, these experimental techniques need transparent surfaces, but the opacity of the textile surface does not allow this type of measurments (Ben Abdessalem, Durand, Akesbi, Chakfe, & Kretz, 2005).

Previous computational studies of vascular grafts have focused exclusively on the hemodynamic of end-to-side configurations without considering the presence of the graft wall (Clement, 2006; Tura, 2003). Several factors are analyzed such as anastomosis angle, graft-to-artery diameter ratio, crimping, anastomosis shape, among others and considering the blood as a homogeneous fluid (Abdessalem, Durand, Akesbi, & Chakfe, 2001; Leuprecht et al., 2002; Probst et al., 2010). However, the type of fabric and properties like permeability and porosity in an anastomoses of end-to-end configurations have not been considered in order to evaluate the influence on local fluid dynamics at several scales of length and that simultaneously consider the plasma flow as well as the motion of individual platelets, related with the graft occlusion.

In summary, the phenomena mentioned above involve a wide range of scales. A computational study would open up the possibilities to explore the multiphysics and multi-scale phenomena around the textile vascular grafts from a biomechanical viewpoint. The goal of this work is to investigate how the type of fabric, permeability and porosity affect both the local fluid dynamics and the fluid-particle interaction among platelets in textile grafts, using a multi-scale approach. This study involves both computational and experimental tests.

Methods

Experimental

The aim of the experimental work is to show the micro-structure and to measure permeability and porosity, according to ISO7198 international standard (*International Standard ISO 7198. Cardiovascular implants-tubular vascular prostheses*, 1998). Two types of samples are analyzed: woven and electrospun samples. The woven grafts are tested with commercial samples and the electrospun samples are manufactured from Poly-Urethane (PU) polymers, using the electrospinning technique, Figure 1. Electrospinning is a common technique used to fabricate micro-nanofibres (Bergmeister et al., 2013). Several manufacturing parameters in the electrospinning technique must be considered such as (Hasan et al., 2014): number of needles, needle size, voltage, speed of collector, needle-collector distance, and flow rate, among others. By varying the parameters, samples with

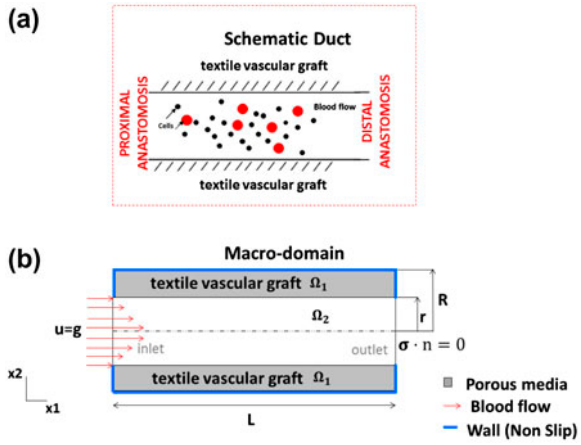

Figure 5. Textile graft at macro-scale: (a) an idealized duct with porous walls, incorporating an end-to-end configuration and release of cells; (b) computational domain.

different porosities, pore size and fiber diameter can be obtained. The principle of fabrication is simple: the samples were manufactured with shape memory polyurethane (Irogran®) 21% w/w in a solution of tehtrahydrofuran (THF) / dimethylformamide (DMF) to 50% w/w at ambient temperature. Later, the solution is charged into a syringe and is pumped at a slow flow rate. A DC voltage is applied to the solution. As the solution travels from the syringe toward the collector, the solvent evaporates and makes a cone shape called the Taylor cone. The collector is wrapped with a sheet of aluminum and sprayed with a mold release agent.

Once the samples were obtained and manufactured, ISO 7198 standard was used for measuring the permeability and porosity of the textile samples (FDA, 2012; Dieval et al., 2001; *International Standard ISO 7198. Cardiovascular implants-tubular vascular prostheses*, 1998). The porosity test determines the area of the voids of the sample. Two methods are used: gravimetric porosity and microscopic porosity. The gravimetric method measures mass per unit area of the sample based on density and wall thickness of the sample:

$$\text{Porosity} = 100 \times \left(1 - \frac{\text{mass}}{\text{area} \times \text{thickness} \times \text{density}}\right) \quad (1)$$

The microscopic method shows the micro-structure and measures the mean of pore size, diameter of the filaments, filament spacing, etc. based on Scanning Electron Microscope (SEM). An analytical balance (model AX200, Shimadzu) and a Scanning Electron Microscope (Phenom) are used for these tasks. Additionally, the wall thickness is measured with a digital micrometer (Mitutoyo).

On the other hand, the water permeability test measures the hydraulic conductivity [(mL/min)/cm^2], which is a measure of water through a given area of the sample prosthesis under a given hydrostatic pressure. Hydraulic conductivity is computed from the equation:

$$\text{Hydraulic conductivity} = \frac{\text{flow rate}}{\text{area}} \quad (2)$$

For this test, a vertical column of water is used with hydrostatic pressure values in the range of 80–150 mmHg, Figure 2. The area of the sample must be between 0.5 and 1.0 cm^2, according to the international standard. Distilled water is used to avoid blocking of the pores. The international standard recommends that leaks around the sample are not observed.

Then, given the value of hydraulic conductivity, permeability can be calculated as follows:

$$k = K \frac{\mu}{\rho g} \quad (3)$$

where k is permeability [m^2], K is hydraulic conductivity [m/s], μ is the dynamic viscosity of the fluid [kg/(m·s)], ρ is the density of the fluid [kg/m^3], and g is the gravity [m/s^2].

Computational

In order to compute the permeability via computational methods, representative volume elements (RVEs) or unit cells of the micro-structure of textile grafts are modelled based on the geometric data obtained from SEM micrographs. Representative unit cells are considered for the small-scale simulations, taking advantage of the periodicity of the textile geometry. In this work, Fabric Mechanics® software was used for the creation of a virtual model of woven sample (Veit, 2012; Wang, 2012) and Rhino® with Grasshopper® software for modelling of an electrospun sample. Once the virtual textile models are made, the models are meshed and can be used as direct input for the flow solver. Then, the Stokes equation is iteratively solved by FEM in those micro-domains and once convergence is reached, using the pressure and velocity fields, the permeability is computed through back substitution of Darcy's law (Ngo & Tamma, 2001):

$$<\mathbf{u}> = -\frac{1}{\mu}\mathbf{k} <\nabla p> \quad (4)$$

with <·> is the average value. A summary of the process is presented in Figure 3.

The micro-scale permeability and porosity are input for flow simulations on the macro-scale.

Later, a set of two numerical cases is described in this work. The textile wall is considered as a porous media with two scales of length: straight tubular structure with porous walls for the macro-domain and representative unit cells of fabric for the micro-domain. A FEM solver in Comsol® is used to solve the flow in laminar conditions for both domains. The numerical process is based on a multi-scale approach, where the fluid flow is solved with the Finite Element Method and the discrete particles are solved with Molecular Dynamic Method. In fact, the equations of fluid flow are solved and a steady state solution of flow is first obtained. Then, the set of equations which describe particle trajectories are solved based on the stored velocity field. The particle position is computed using a Lagrangian approach based on a Newtonian formulation by a time dependent solver. The drag and gravity forces were considered. Moreover, a mesh independence tests were performed for each model both in macro-domain and in micro-domain. Only results from fine meshes are presented. The Finite Element Discretization method in Comsol® is the Galerkin method in which a weak

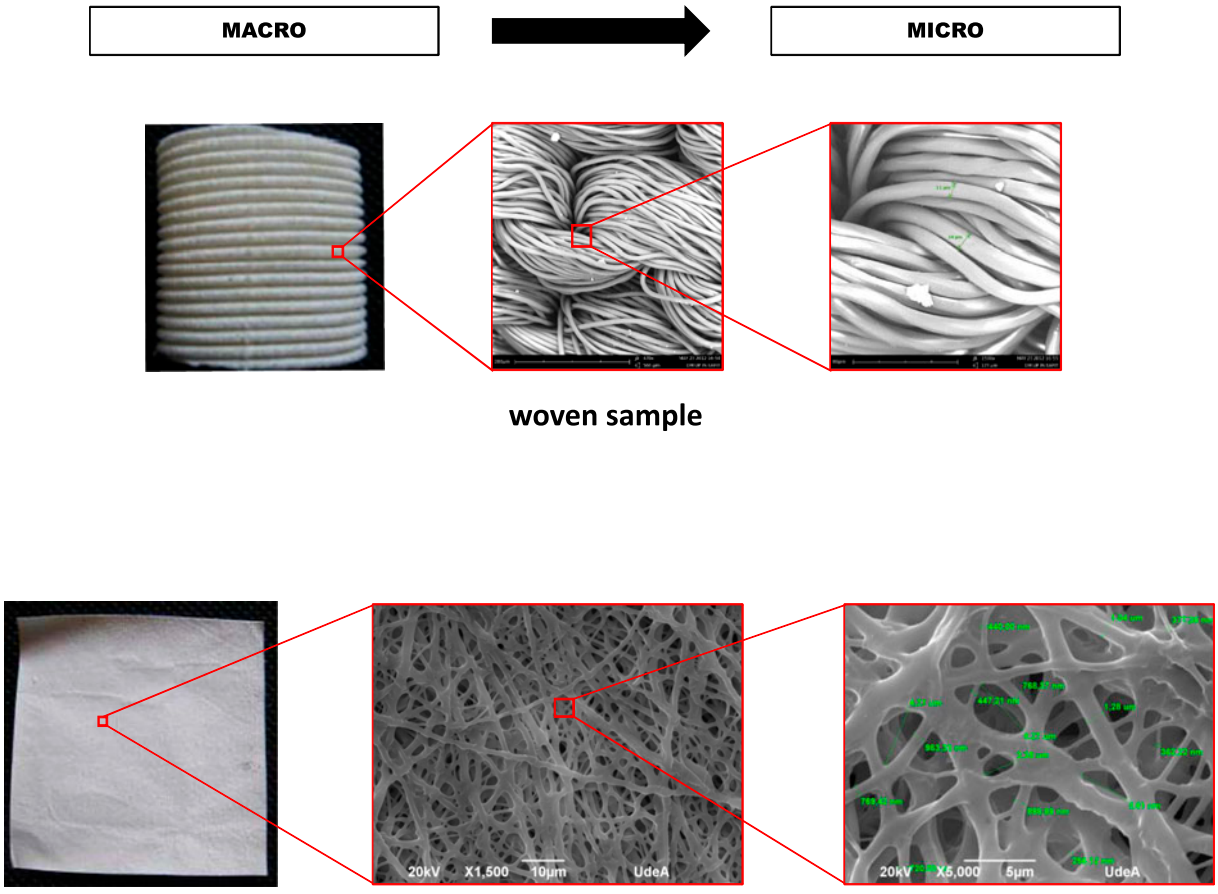

Figure 6. SEM micrographs of the textile grafts: woven sample (top) and electrospun sample (bottom).
Notes: Scale bar for woven sample: 280 and 80 μm. Scale bar for electrospun sample: 10 and 5 μm.

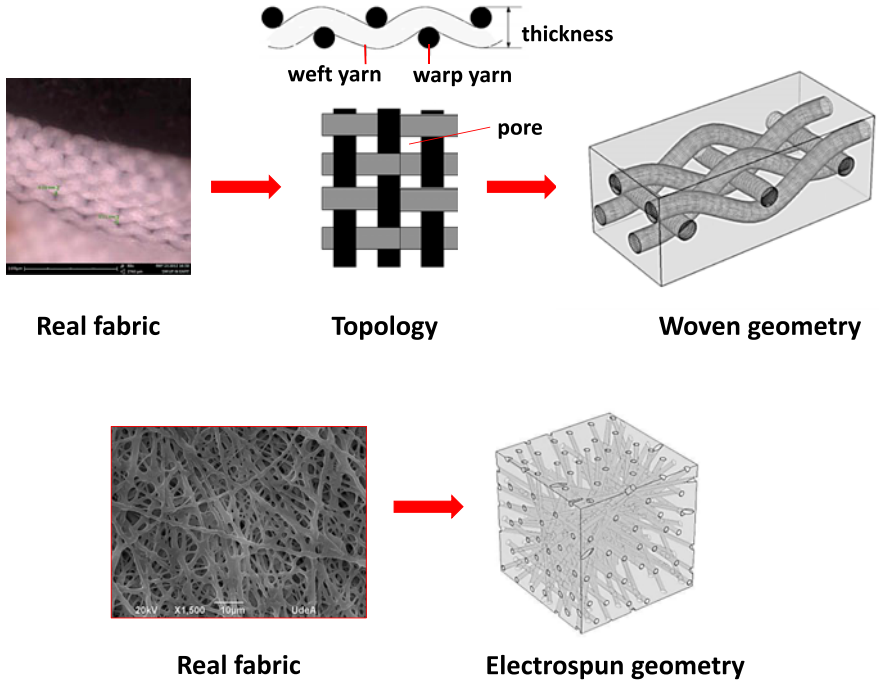

Figure 7. 3D geometric representations of textile grafts: woven geometry (top) and electrospun geometry (bottom).

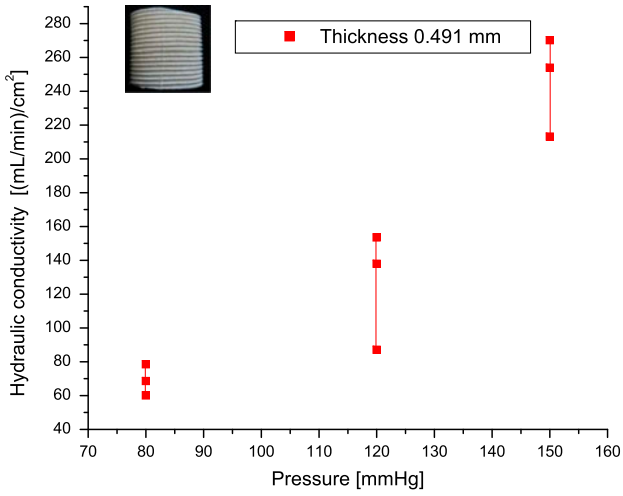

Figure 8. Experimental hydraulic conductivity [(mL/min)/cm^2] values with hydrostatic pressure values at 80, 120 and 150 mmHg for the woven sample.

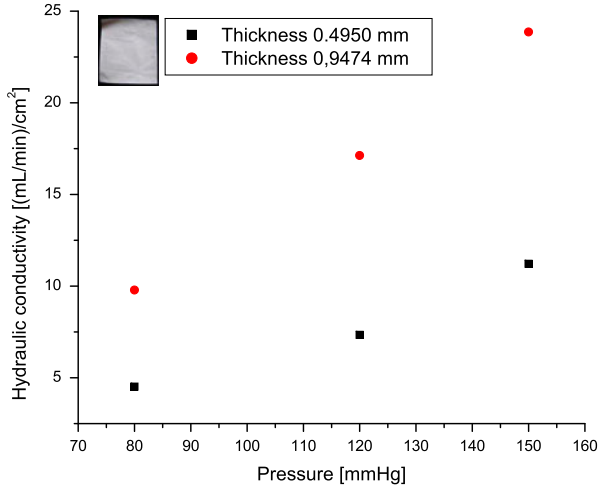

Figure 9. Average of experimental hydraulic conductivity [(mL/min)/cm^2] values with hydrostatic pressure values at 80, 120 and 150 mmHg for electrospun samples.

equation form corresponding to a strong equation is obtained by multiplying with the basis function and integrating over the computational domain. Lastly, the fluid-particle interaction is accomplished in one-way.

Governing equations

Model considerations

Due to the complex interaction of all the physical and chemical processes taking place between the blood and the textile vascular graft, it is necessary to consider some simplifications and assumptions in order to computationally solve the problem. The model simplifications and assumptions are as follows:

- The effect of the wall motion is considered neglected. Synthetic grafts are generally stiffer than the native vessels (Tura, 2003).
- There are several challenges when attempting to model the behavior of the blood flow from a biomechanical viewpoint (Tura, 2003). The blood is not merely a continuum fluid, but it is composed of various cellular components and proteins. Additionally, when an artificial wall of the graft is first exposed to blood, a process of activation, adhesion and aggregation of platelets will begin, which may form a platelet plug that occludes the graft. Furthermore, the presence of clots may alter the physiological transport and the local environment of the graft, reducing the flow and causing a restriction in blood supply to the textile wall. Occlusion of a graft often results in hospital re-admission and re-operation for the patient. Hence, the blood is considered as a suspension of platelets in plasma, related with the graft occlusion. Blood plasma is an aqueous solution that can be assumed Newtonian, homogeneous and incompressible with real blood properties: $\rho = 1.056\,\mathrm{g/cm^3}$, $\mu = 3.5\,\mathrm{cPoise}$ and $\nu = 0.035\,\mathrm{cm^2/s}$ (Abdessalem et al., 2001; Clement, 2006).
- The platelets are considered as micro-particles due to their small size. The platelets are the smallest of blood cells, 2 to 3 microns in size (Clement, 2006; Grinberg et al., 2011).
- Chemical interactions and the influence of the electric charge of the cells are not considered.

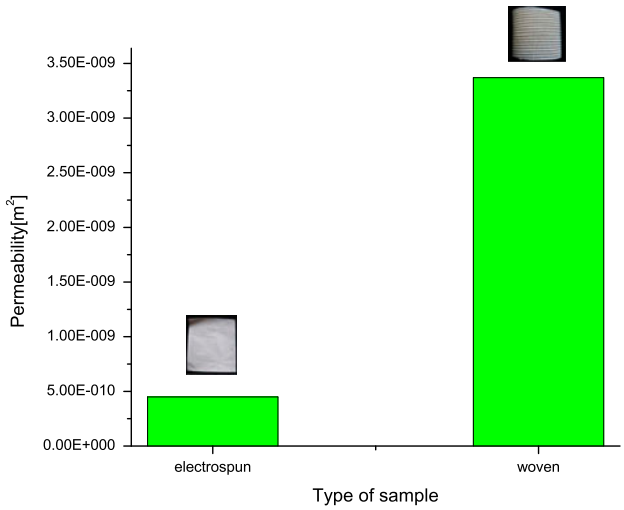

Figure 10. Experimental permeability [m^2] values according to Equation (3) for woven and electrospun samples.
Notes: The thickness and porosity were 0.9474 mm and 71.99% for the electrospun sample and 0.491 mm and 80.89% for the woven sample.

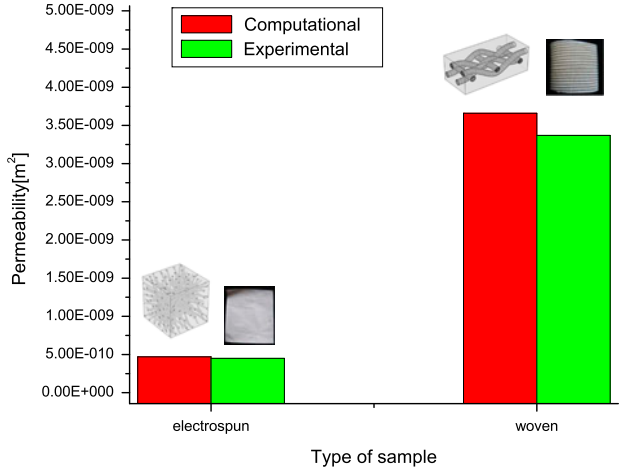

Figure 11. Experimental permeability [m^2] values according to Equation (3) and computational permeability [m^2] values for woven and electrospun samples.

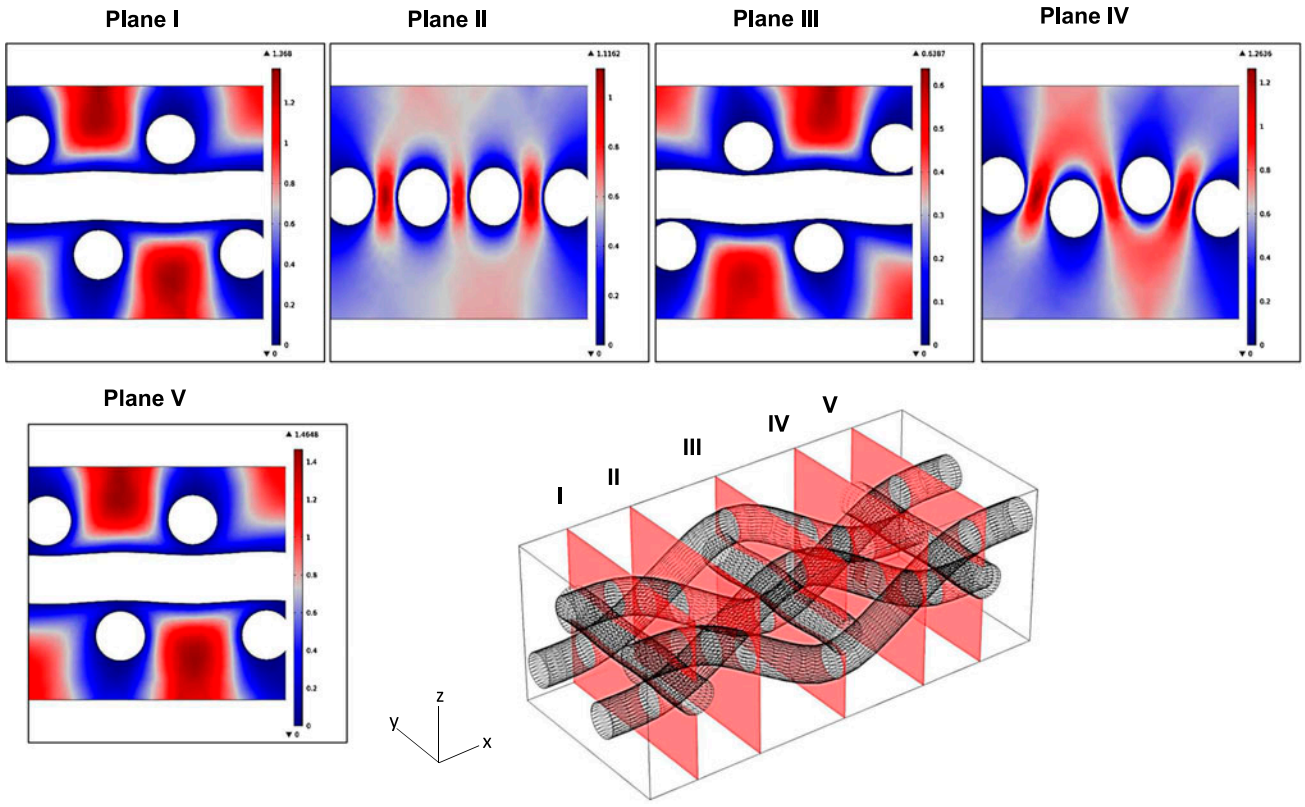

Figure 12. Velocity magnitude for five cross-sections at different locations within the unit cell of the woven sample.
Note: The velocity scale is from 0.0 (blue) to 1.368 mm/s (red). The weave porosity is 0.8258 and the permeability is 1.14e-9 [m^2]. The applied pressure gradient drives flow in the *z*-direction.

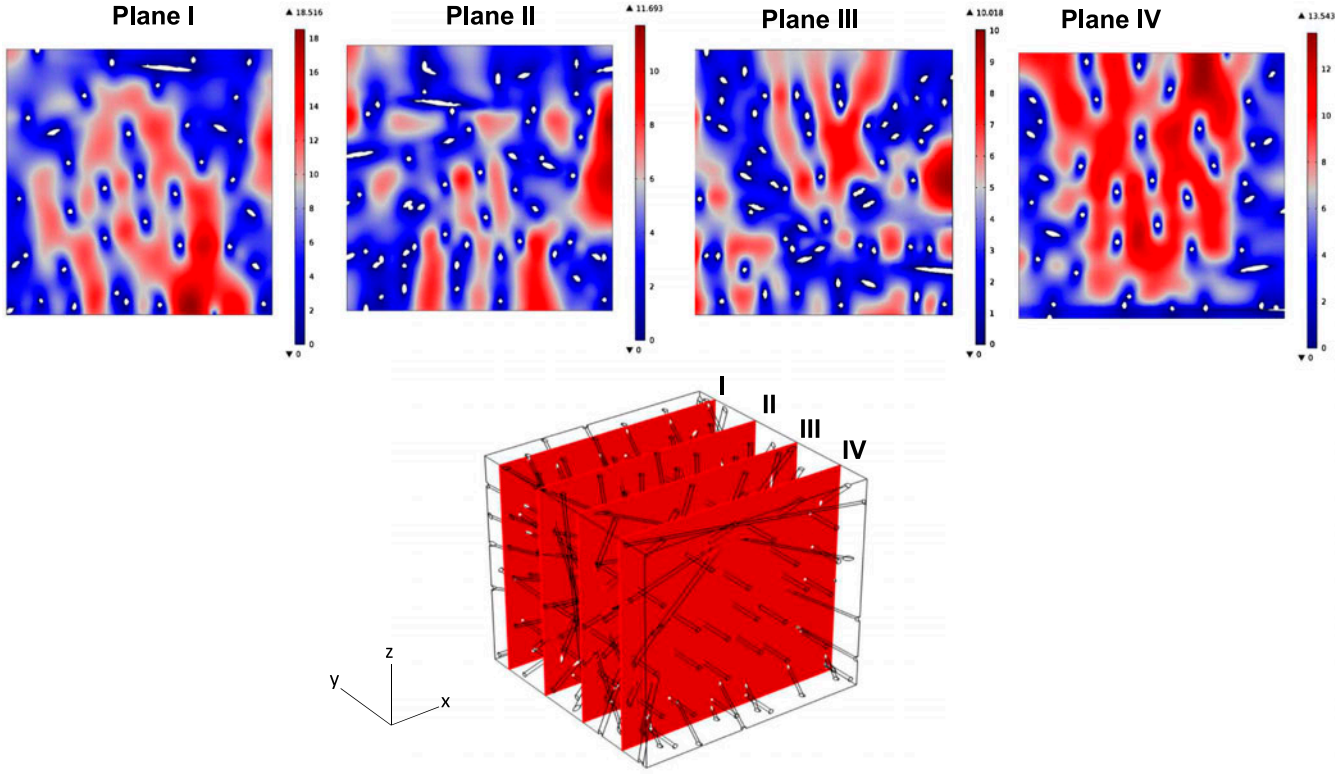

Figure 13. Velocity magnitude for four cross-sections at different locations within the unit cell of the electrospun sample.
Notes: The velocity scale is from 0.0 (blue) to 18.516 mm/s (red). The electrospun porosity is 0.9668 and the permeability is 4.7012e-10 [m^2]. The applied pressure gradient drives flow in the z-direction.

- Magnus effect is considered negligible, so that there are no particle rotational effects.
- The porous domains are saturated by the moving fluid, so that there are no capillarity effects.

For the purpose of modelling the behavior between a textile vascular graft and the blood at several length scales, treating blood as a suspension of cells in plasma, different mathematical models are required for each scale.

Blood flow for micro-scale

As was mentioned before, representative unit cells of the textile wall are considered for the description of internal structure of the micro-domains, due to the periodicity of the textile geometry. Two configurations are included: woven and electrospun samples, Figure 4.

Usually in a micro-fluidics system, the flow of the carrier fluid is assumed to be steady and with low Reynolds (Vafai, 2011). Hence, the system is modeled by the steady Stokes equations:

$$\nabla \cdot \mathbf{u} = 0 \tag{5}$$

$$0 = -\nabla p + \mu \triangle \mathbf{u} + \mathbf{F} \tag{6}$$

Blood flow for macro-scale

In this case, it is considered a straight tubular structure as the domain of an anastomoses of end-to-end configuration on a large scale. The macro-domain of Figure 5 includes a two-dimensional duct of length L, with porous walls located at $y = \pm r$. Fluid will be injected into the duct at $x = 0$, having a parabolic velocity profile and with a given distribution of particles. It is prescribed a free stress condition at the outlet.

It is necessary to solve the flow in both the textile and the fluid regions (domain decomposition). The flow in the vascular graft can be modelled as free flow in the internal duct (Ω2) and flow through porous media in the textile (Ω1). The field of free flow is described by the conventional Navier–Stokes equations and the interstitial flow passing through textile graft pores is described by Brinkman's equation (Comsol, 2012; Ehrhardt, 2010).

In the free flow:

$$\nabla \cdot \mathbf{u} = 0 \tag{7}$$

$$\rho \frac{\partial \mathbf{u}}{\partial t} + \rho \mathbf{u} \cdot \nabla \mathbf{u} = -\nabla p + \mu \triangle \mathbf{u} + \mathbf{F} \tag{8}$$

In the porous media, the system is assumed as a homogeneous medium with a specified porosity and permeability:

$$\nabla \cdot \mathbf{u} = 0 \tag{9}$$

$$\frac{\rho}{\varepsilon}\frac{\partial \mathbf{u}}{\partial t} + \frac{\rho}{\varepsilon}\left[(\mathbf{u} \cdot \nabla)\frac{\mathbf{u}}{\varepsilon}\right] = -\nabla p + \frac{\mu}{\varepsilon}\triangle \mathbf{u} - \frac{\mu}{k}\mathbf{u} + \mathbf{F} \tag{10}$$

where $\mathbf{u}$ and p are the superficial velocity and the pressure, ρ and μ are the fluid density and fluid dynamic viscosity, ε and k are the porosity and permeability of the porous media, and $\mathbf{u}/\varepsilon$ is called interstitial velocity, Darcy velocity or filtration velocity. Furthermore, ε and k are defined for the macro-domain based on the results that are obtained by experimental and computational methods from the micro-domain.

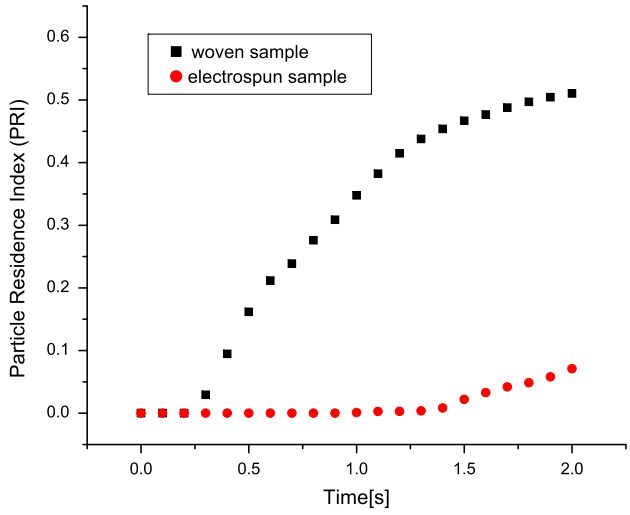

Figure 14. Particle Residence Index (PRI) for woven and electrospun samples in the outlet side.
Notes: PRI for this case is defined as the ratio of the number of particles which reach the outlet divided by the number of particles released. A total of 3000 particles were initially released at $t = 0$.

Cellular transport

The kinematics of a cell in the Eulerian–Lagrangian framework may be written as (Clement, 2006; Yang, Ding, York, & Broeckx, 2008):

$$m_p \frac{\partial(\mathbf{v}_p)}{\partial t} = \mathbf{F}_{\text{drag}} + \mathbf{F}_{\text{g}} + \mathbf{F}_{\text{ext}} \tag{11}$$

where a particle is defined by its diameter d_p, its mass m_p or density ρ_p and its velocity $\mathbf{v}_p$. In this work, the particles have been defined using the properties of platelets, related with the graft occlusion. The initial position of the particles was selected at the centroid of each element surrounding the nodes in a FEM mesh. This decomposition has a fixed mesh for fluid and rigid particles which can freely move.

The first term of the surface forces is the hydrodynamic drag force, which is calculated as (Vallier, 2010):

$$\mathbf{F}_{\text{drag}} = -m_p \frac{(\mathbf{u} - \mathbf{v}_p)}{\tau_p} \tag{12}$$

where $\mathbf{u}$ is the velocity of the fluid and the mass of the particle m_p, assuming that the particle is spherical, is defined as:

$$m_p = \frac{1}{6}\rho_p \pi d_p^3 \tag{13}$$

Particle's relaxation time τ_p or momentum response time is the time it takes for a particle to respond to changes in local flow velocity:

$$\tau_p = \frac{4}{3}\frac{\rho_p d_p}{\rho_f C_D \mid \mathbf{u} - \mathbf{v}_p \mid} \tag{14}$$

The friction coefficient C_D for spherical particles is defined as follows:

$$C_D = \begin{cases} \frac{24}{Re_p} & \text{if } Re_p < 1 \\ \frac{24}{Re_p}\left(1 + \frac{1}{6}Re_p^{2/3}\right) & \text{if } 1 \le Re_p \le 1000 \\ 0.44 & \text{if } Re_p > 1000 \end{cases} \tag{15}$$

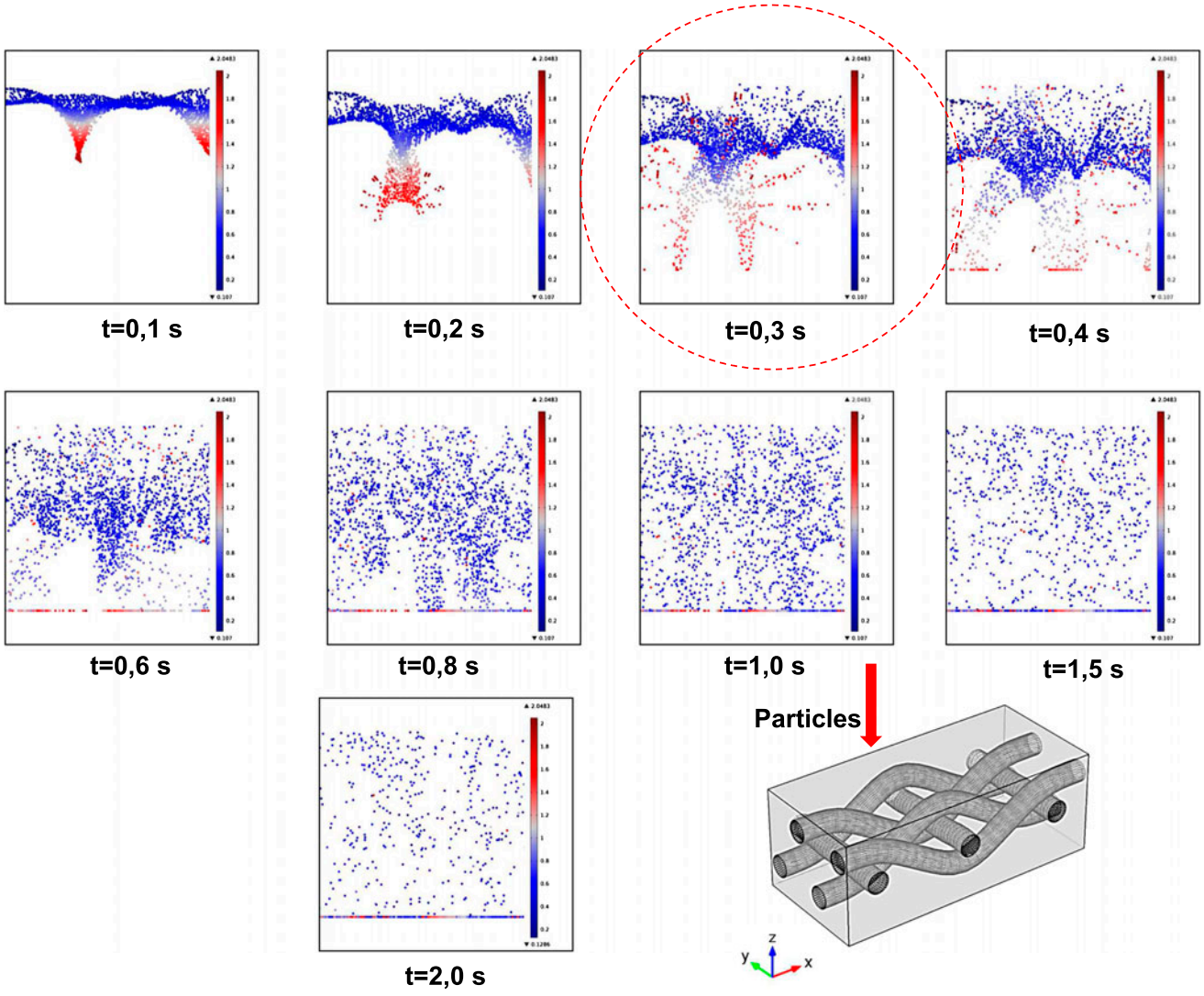

Figure 15. Plot of particle trajectories inside the woven wall.
Note: The color is the particle velocity magnitude from 0.0 to 2.0483 mm/s. The circle highlights the number of particles which reach the outlet at 0.3 s.

Thus, C_D is a function of the particle Reynolds number:

$$Re_p = \frac{\rho_f \, d_p \mid \mathbf{u} - \mathbf{v}_p \mid}{\mu_f} \tag{16}$$

The second term in the Equation (11) represents a combination of the buoyancy and gravitational forces acting on the particle (Clement, 2006; Yang et al., 2008):

$$\mathbf{F}_g = \frac{4}{3}(\rho_p - \rho_f)\pi \frac{d_p}{2}\mathbf{g} \tag{17}$$

The third term in the Equation (11) represents external forces. These forces may be due to attraction of cells to nutrients in the blood, adhesive forces among platelets and the artificial surface (i.e. textile wall), or aggregating forces among platelets, among others.

Lastly, treating blood as a suspension of cells in plasma, the low concentration of platelets in the blood allows for the transport of these cells to be computed in a one-way coupling, i.e. fluid-to-particle forces are transferred to the particles but these particles do not affect flow field momentum (Onate et al., 2014; Vallier, 2010). Indeed, a normal range of red blood cells counts for healthy adults is between 4.2 and 6.7 million per microliter of blood, whereas that a normal range of platelets is between 150.000 and 400.000 per microliter (Clement, 2006).

Table 1. Parameters of the Electrospinning Process.

Parameters	Values
Number of needles	10
Needle size (gauge):	21
Voltage [kV]:	14
Speed [rpm] of mandrel: approx.	36
Needle-mandrel distance [cm]:	14-16
Flow rate [ml/h]:	0.25

Results and discussion

This section is organized as follows: computational reconstruction of the textile samples, characterization of permeability and porosity using both computational and experimental methods,

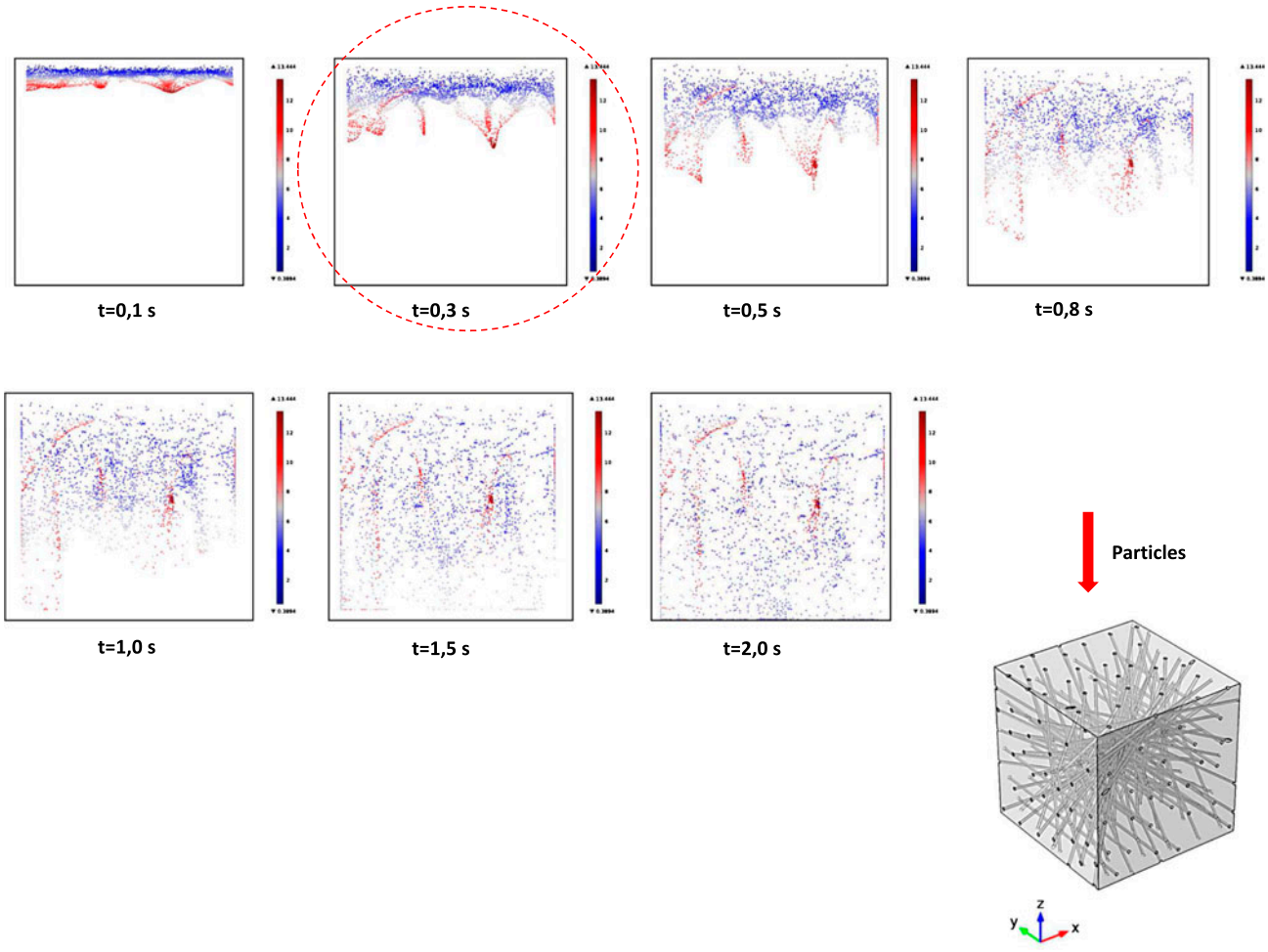

Figure 16. Plot of particle trajectories inside the electrospun wall.
Note: The color is the particle velocity magnitude from 0.0 to 13.44 mm/s. The circle highlights the number of particles that do not reach the outlet at 0.3 s.

and two numerical cases for the macro-domain and micro-domain.The flow pattern and the cellular transport of individual platelets is described in textile vascular grafts with an anastomoses of end-to-end configuration, for both macroscopic and microscopic viewpoints. The effect of two different types of fabrics was evaluated considering the pass of fluid and particles through the porous walls. A mesh independence tests were performed for each model both in macro-domain and in micro-domain within 5% relative error. Only results from fine meshes are presented.

Computational reconstruction of the textile samples

As was mentioned before, two types of samples were analyzed: woven and electrospun. The woven sample was a straight tube of polyester with 8 mm of diameter. The linear density of longitudinal (warp) yarns is 110 dtex and the linear density of transversal (weft) yarns is 167 dtex. The electrospun samples were manufactured with thickness values in the range of 82–1000 μm. This range was considered based on both the thicknesses of commercial specifications of grafts and vessel walls. By measuring over 20 SEM images, it was found that the filament diameters of the electrospun mats varied from 250 nm to 2.4 μm and the pore sizes varied from 1.1 to 4.3 μm. Some parameters of the electrospinning process are listed in Table 1.

Once the samples were obtained and manufactured, micrographs from SEM were analyzed in order to obtain a geometric description and variability of the micro-structure inside the textile wall, Figure 6. The fabric type, thickness, number of layers, volume fraction, yarn dimensions and spacing in between the yarns, among others properties were measured in order to develop an accurate and appropriate virtual textile model.

Figure 7 shows 3D geometric representations of the micro-structure of fabric, both for woven and electrospun samples, based on data from SEM micrographs. For instance, to create the woven unit cell, the cell topology was defined by the thickness, number of layers and weft and warp yarn pattern. To create the electrospun unit cell, cylindrical and straight filaments of constant diameter are randomly placed in a cubic domain with free overlapping based on the volume fraction, thickness, diameter and length. These CAD models were used in simulations to predict permeability and blood-material interaction for the micro-domain.

Characterization of permeability and porosity

The purpose of this section is to evaluate the permeability and porosity both for the real samples and the virtual models. The first part presents the characterization of permeability and porosity by experimental methods, according to the ISO 7198

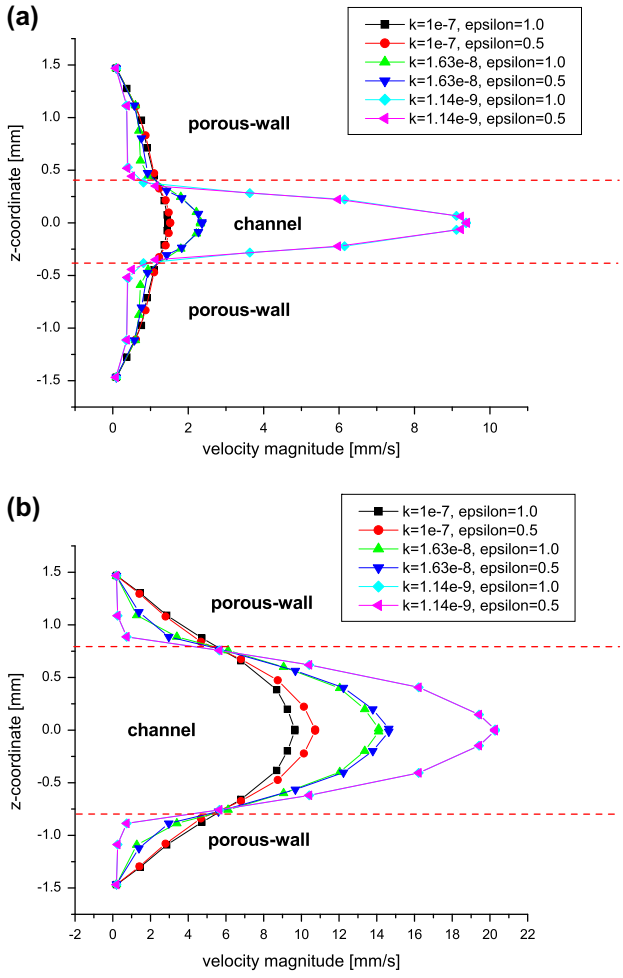

Figure 17. Cross section of velocity field (velocity magnitude in mm/s) in the middle of the duct with different radius, permeabilities and porosities. (a) Radius = 355 μm; (b) Radius = 900 μm.

standard. The last part predicts the permeability and porosity for the representative volume elements (RVE) of virtual models by computational methods. Permeability is computed through back substitution of Darcy's law using the computed pressure and velocity fields.

Experimental method

Hydraulic conductivity [(mL/min)/cm^2] was first evaluated, which is a measure of water which can flow through a circular sample, with an area of 1 cm^2 under physiological pressure conditions. Figure 8 shows some hydraulic conductivity values of the woven sample, in the range of 50–300 (mL/min)/cm^2. Thickness and porosity were 0.491 mm and 80.89%. According to literature Greenhalgh and Dunn (1998) and Tura (2003), these results for woven fabrics were within the same range as those studies (i.e. less to 1000 (mL/min)/cm^2).

For electrospun samples, hydraulic conductivity values were obtained in the range of 4–24 (mL/min)/cm^2, Figure 9. The thickness and porosity were 0.4950 mm and 63.41% for the sample 1 and 0.9474 mm and 71.99% for the sample 2. Polyurethane samples were within the range of less than 30 (mL/min)/cm^2, corresponding to this type of materials, according to literature Tura (2003).

Once hydraulic conductivity was obtained, permeability was calculated based on Equation (3), see Figure 10. The difference between the electrospun and woven samples is probably related to the complex micro-structure of the electrospun sample that was observed by SEM, producing a greater resistance to pass through the textile wall.

Computational method

Then, simulations were performed for woven and electrospun samples in order to calculate permeability via computational methods. Thickness and porosity were 1 mm and 96.68% for the electrospun virtual model and 0.45 mm and 82.58% for the woven virtual model. Although the porosity in the electrospun sample was greater than the woven sample, the electrospun micro-structure was more complex, causing greater resistance to the flow and lower permeability values, Figure 11. This influence of the micro-structure possibly affects the mass transport and its ability for cells and nutrients to penetrate the wall.

Lastly, comparing experimental and computational data, it is possible to observe that the results have the same trend within a similar range, with a relative error of 4.65% for the electrospun sample and 8.53% for the woven sample, Figure 11. The discrepancies between experimental and computational results can perhaps be attributed to slight differences in the unit cell micro-structure dimensions.

Numerical cases

The aim of these numerical cases is to study the flow pattern and the fluid-particle interaction for both the macro-domain and the micro-domain. For the macro-domain (i.e. a straight tubular structure with porous walls), the effect of parameters as the permeability, porosity and the duct-diameter were analyzed. For the micro-domain (i.e. woven and electrospun virtual models), the effect of the type of textile fabric was analyzed. The velocity

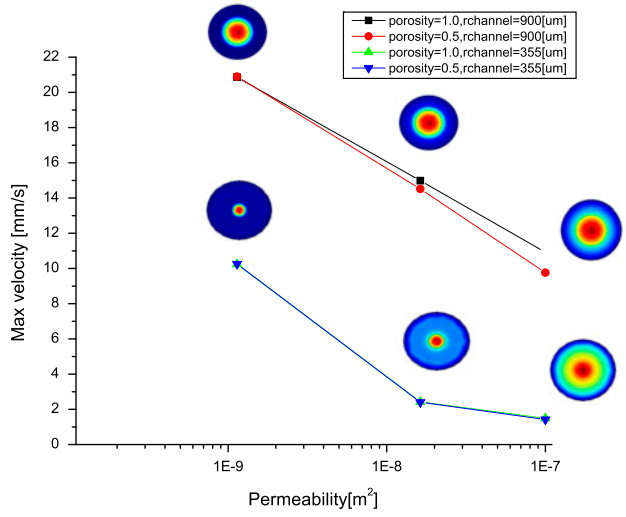

Figure 18. Maximum velocity [mm/s] vs. permeability [m^2] of the wall with different radius, permeability and porosity. *X*-axis is in $\log_{10}$.
Notes: Contours of the velocity magnitude corresponding to a cross section in the middle of the duct.

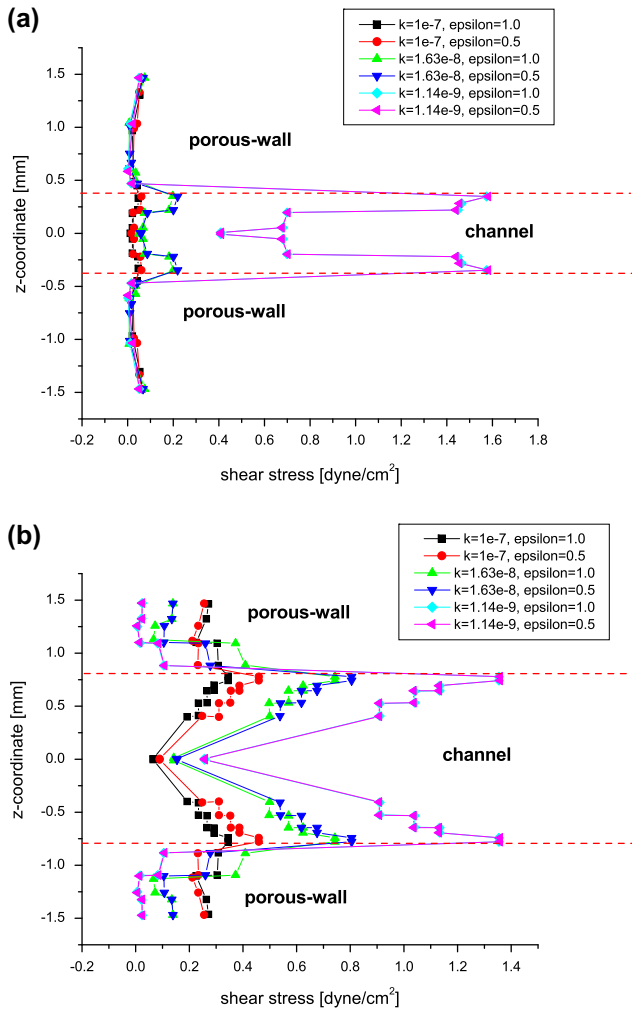

Figure 19. Cross section of the shear stress [dyne/cm^2] in the middle of the channel with different radius, permeabilities and porosities. (a) Radius = 355 μm; (b) Radius = 900 μm

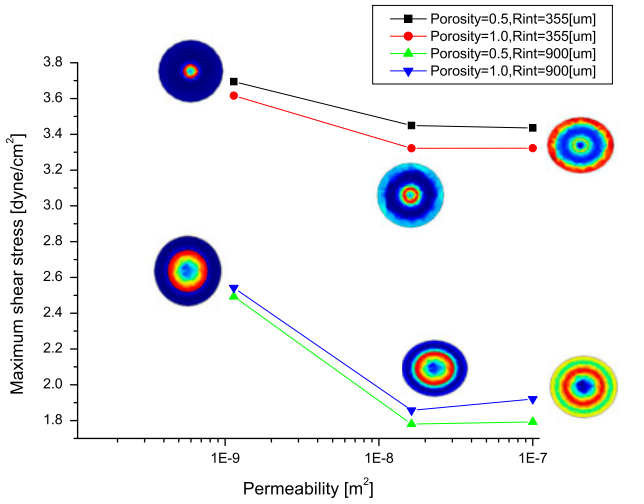

Figure 20. Maximum shear stress [dyne/cm^2] vs. permeability [m^2] with different radius, permeability and porosity. *X*-axis is in $\log_{10}$.
Note: Contours of shear stress corresponding to a cross section in the middle of the channel.

field and particle residence index (PRI) were computed. PRI is an indicator used to measure how long a group of particles remains in a zone.

Micro-Scale: woven and electrospun samples

Effect of the type of textile fabric. Simulations were initially carried out for a unit cell of woven sample. The unit cell is composed of perpendicular yarns aligned along the x and y axes, which are interwoven to form a woven fabric. A normal pressure gradient of 1Pa/m was applied to the plane of the fabric (in the z-direction) and fluid flow was simulated through the unit cell. The pressure gradient was selected to set the flow in low Reynolds number regime. Moreover, periodic boundaries were used in the other directions, equivalent to simulating flow through an infinite fabric. As shown in Figure 12, plane sections I, III and V represent the flow which is blocked by the yarns. Plane sections II and IV represent planes located between two lines of yarns and show lower flow resistance, where the flow has a direct path through the wall. As a result, this significant flow between two adjacent yarns defines a high permeability zone. The top and bottom walls of the yarns are a favorable area for cells to adhere due to the lower flow velocity levels. In contrast, there are relatively high local velocities between two strands of yarns, so the cells would have more likelihood to be washed out the wall.

On the other hand, the porous structure in the electrospun sample is complex, and complicated flow patterns are observed as shown in Figure 13. The velocity magnitude is higher in the narrowest pores and tends to decrease where the pore channel size increases. Moreover, there is a considerable zone with low flow velocity levels, possibly because of the increase of the pore path (tortuosity) and implying that this area would be suitable for cell attachment and deposition, Figure 13 (plane sections II and III). However, plane sections I and IV have a larger pore size with low resistence to flow (i.e. high permeability).

Table 2 summarizes some of the properties of the samples studied and their computational results: average velocity [mm/s], average shear stress [dyne/cm^2] and permeability [m^2] values. Although the electrospun sample has higher porosity values than the woven sample, its micro-structure is more complex with higher surface area values, causing lower values of permeability and lower values of particle residence index, Figure 14. A total of 3000 particles were initially released at $t = 0$.

The electrospun sample presents higher PRI values than the woven sample. This means that is more likely for the electrospun sample that the cells remain trapped increasing the agregation and deposition of platelets, Figures 15 and 16.

Macro-Scale: straight tubular structure with porous walls

Effect of permeability, porosity and duct diameter on local fluid dynamics. The velocity profile for the macro domain, described in Figure 5 along a vertical cross section in the middle of the duct, is depicted in Figure 17. The plot shows a parabolic profile with the existence of radial velocity gradients across the interface between the porous wall and the free duct.

It also shows that the axial flow rate in the duct is reduced as permeability is increased, Figure 18. This behavior occurs for both diameters. Moreover, there is also a slight variation when porosity is modified. In general, this behavior indicates the tendency of the fluid to move towards the porous walls because of leakage flow, causing deviations from Poiseuille flow.

Table 2. Properties and computational results of the samples studied: porosity, specific surface area, average velocity, average shear stress and permeability.

Sample	Porosity	Specific surface area [mm^2]	Average velocity [$\frac{mm}{s}$]	Average shear stress $\frac{dyne}{cm^2}$	Permeability m^2
Woven	0.8258	255.0	0.7251	0.5156	1.14e-9
Electrospun	0.9668	1243.3	4.6525	0.3265	4.70e-10

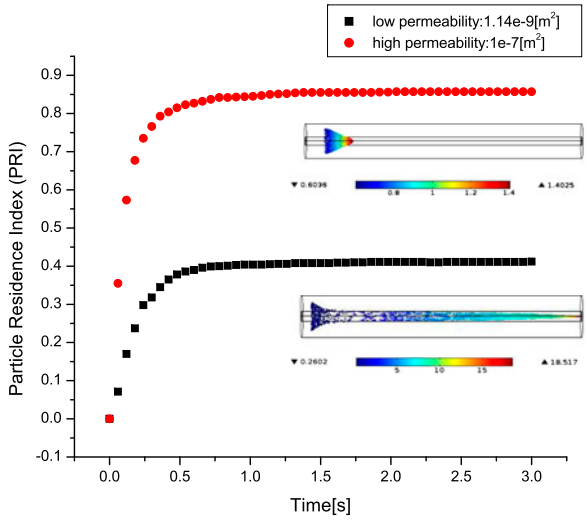

Figure 21. Time evolution of PRI in the porous wall (i.e. number of deposited particles inside the wall divided by the total number of initially released particles). Notes: Duct radius is 355 [um]. Particles were visualized for 3 s. The color scale represents the magnitude of particle velocity in mm/s.

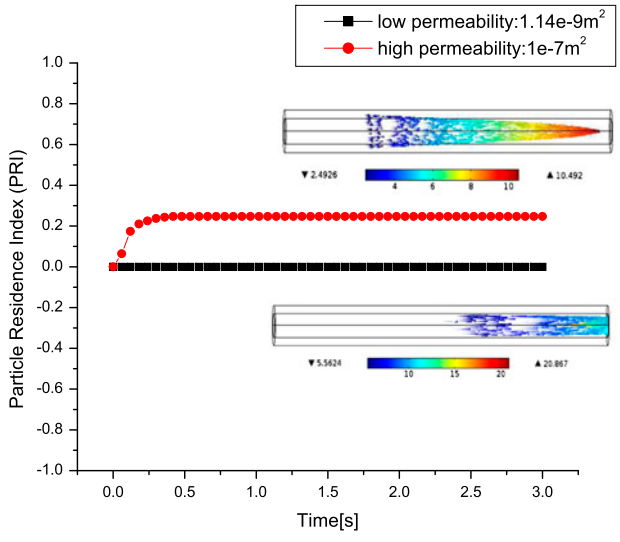

Figure 22. Time evolution of PRI in the porous wall (i.e. number of deposited particles inside the wall divided by the total number of initially released particles). Notes: Duct radius is 900 [μm]. Particles were visualized for 3 s. The color scale represents the magnitude of particle velocity in mm/s.

The hemodynamic conditions inside the textile graft lead to the development of superficial stresses near the wall due to blood flow. Usually, a linear shear stress curve characterizing Poiseuille flow is obtained for a Newtonian fluid in tubular vessels. However, porous walls cause different local characteristics as shown in Figure 19.

Figure 20 shows that shear stress is reduced as permeability is increased. As mentioned before, the presence of low shear stress is frequently associated by stagnant points and can induce an excessive deposition of platelets over the wall.

Effect of permeability, porosity and duct diameter on cellular transport. A total of 1000 particles were initially released at $t = 0$. The first particles reached the outlet at around 3 s. The wall with high permeability (i.e. 1e-7m^2) had a PRI of 85.7%, i.e. number of deposited particles inside the wall divided by the total number of initially released particles, Figure 21. On the contrary, the wall with low permeability (i.e. 1.14e-9 m^2) had a PRI of 41.2%. With leakage flow through the porous wall, the particles move to the wall, increasing the residence time. This fact would increase the probability of platelet deposition and aggregation inside the wall.

For the case of the duct with radius of 900 um, the wall of high permeability (i.e. 1e-7 m^2) had a PRI of 24.7%, while the wall of low permeability (i.e. 1.14e-9 m^2) had a PRI of 0%, Figure 22.

Conclusions

The results have shown that the type of fabric in textile vascular grafts and the degree of porosity and permeability affect the local fluid dynamics and the level of penetration of platelets through the graft wall, thus indicating their importance as design parameters. It was found during the simulations that the variability of permeability is strongly depended on the micro-structure of the fabric, changing the local dynamics of fluid and the time of residence of platelets inside the wall. For instance, although the electrospun sample had higher porosity values than the woven sample, its micro-structure was more complex, causing lower permeability values, lower PRI values, and increasing the likelihood that the platelets to be aggregated and deposited within the wall. From macroscopic viewpoint, the presence of a porous wall along a channel causes deviations from Poiseuille flow due to leakage flow through the wall. The axial flow rate and the shear stress are reduced in magnitude as the permeability is increased and this behavior is even observed for different diameters and porosities. Moreover, with leakage flow through the porous wall, the particles move to the wall, increasing the residence time.

Although the proposed model seems to be useful in evaluating the macro and micro-flow pattern and the fluid-particle interaction among platelets considering the type of fabric of a textile graft, an important future work would be: extend the work to other type of textile vascular grafts and topologies, and experimental tests to evaluate and validate how change the porosity and permeability over time due to the penetration and deposition of cells like platelets, endothelials and fibroblasts.

With these developments, the proposed work would contribute with more details to the understanding of this research.

In conclusion, the development of new textile grafts may be improved if details of the flow pattern and the mobility of blood cells through the graft wall are known and predictable, before the graft is manufactured.

Acknowledgements

I would also like to thank to Dr. Lina Hoyos (UPB) for their collaboration and advice on experimental tests, to Camilo Andrés Páramo (UPB) for his collaboration and advice on electrospun CAD models, to Mauricio Arroyave (EAFIT) for his collaboration on SEM micrographs.

Disclosure statement

No potential conflict of interest was reported by the authors.

Funding

This work was supported by Universidad Pontificia Bolivariana and Universidad Eafit.

ORCID

John Bustamante http://orcid.org/0000-0002-4855-9896

References

Abdessalem, S. B., Durand, B., Akesbi, S., & Chakfe, N. (2001). Blood flow in a polyester textile vascular prosthesis: Experimental and numerical study. *Textile Research Journal, 71*(2), 178–183. doi:10.1177/004051750107100214

Ben Abdessalem, S., Durand, B., Akesbi, S., Chakfe, N., & Kretz, J. G. (2005). Fluid-structure interaction in a free end textile vascular prosthesis. *The European Physical Journal Applied Physics, 31*(3), 211–216. doi:10.1051/epjap:2005060

Bergmeister, H., Strobl, M., Grasl, C., Liska, R., & Schima, H. (2013). Tissue engineering of vascular grafts. *European Surgery, 45*, 187–193. doi:10.1007/s10353-013-0224-x

Berthier, J., & Silberzan, P. (2010). *Microfluidics for biotechnology* (2nd ed.). Norwood, MA: Artech House.

Bronzino, J. (2000). *The biomedical engineering. Handobook* (Vol. 2). Boca Raton, FL: CRC Press, Springer, IEEE.

Chlupac, J., Filova, E., & Bacakova, L. (2009). Blood vessel replacement: 50 years of development and tissue engineering paradigms in vascular surgery. *Physiological Research, 58*(2), 119–139.

Cioffi, M., Boschetti, F., Raimondi, M., & Dubini, G. (2006). Modeling evaluation of the fluid-dynamic microenvironment in tissue-engineered constructs: a micro-ct based model. *Biotechnology and Bioengineering, 93*(3), 500–510. doi:10.1002/bit.20740

Clement, K. (2006). *Biofluid dynamics. Principles and selected applications*. Boca Ratón, FL: Taylor and Francis Group.

Comsol (2012, October). *Coupled free and porousmedia flow*. Retrieved from http://www.comsol.com/model/download/39648/porous_free.pdf

Dieval, F., Chakfe, N., Bizonne, S., Magnen, J. L., Beaufigeau, M., Mathieu, D., …Durand, B. (2001). Les tests mechaniques devaluation des protheses vasculaires. *ITBM-RBM Elsevier, 22*(2), 70–87. doi:10.1016/S1297-9562(01)90033-6

Ehrhardt, M. (2010). An introduction to fluid-porous interface coupling. In *Coupled Fluid Flow in Energy, Biology and Environmental Research. Progress in Computational Physics* (Vol. 2), Begische Universitat Wuppertal. doi:10.2174/97816080525471120101

FDA. (2012, May). *Guidance for industry and fda staff: Guidance document for vascular prostheses 510(k) submissions*. Retrieved from http://www.fda.gov/medicaldevices

Greenhalgh, E., & Dunn, M. (1998). *Modeling blood flow through vascular grafts* (Technical Report). National Textile Center Report, Philadelphia College of Textile and Science, Philadelphia, PA. Retrieved from: http://www.ntcresearch.org

Grinberg, L., Morozov, V., Fedosov, D., Insley, J., Papka, M., Kumaran, K., & Karniadakis, G. (2011, November). A new computational paradigm in multiscale simulations: Application to brain blood flow. In *S. Proceedings of 2011 International Conference for High Performance Computing Networking & A* (pp. 1–12). Seattle, WA: IEEE. doi:10.1145/2063384.2063390

Hasan, A., Memic, A., Annabi, N., Hossain, M., Paul, A., Dokmeci, M., …Khademhosseini, A. (2014). Electrospun scaffolds for tissue engineering of vascular grafts. *Acta Biomateria, 10*(1), 11–25. doi:10.1016/j.actbio.2013.08.022

International Standard ISO 7198. Cardiovascular implants-tubular vascular prostheses (1998). International Organization for Standardization, Geneva, Switzerland. Retrieved from: https://www.iso.org/standard/50661.html

Kutz, M. (2003). *Standard handbook biomedical engineering and design*. New York, NY: McGraw-Hill.

Leisen, J., Beckham, H., & Farber, P. (2004). *Microflow in textiles* (Technical Report NTC Project F04-GT05). National Textile Center Annual Report. University Research Consortium. Retrieved from: http://www.ntcresearch.org

Leuprecht, A., Perktold, K., Prosi, M., Berk, T., Trubel, W., & Schima, H. (2002). Numerical study of hemodynamics and wall mechanics in distal end-to-side anastomoses of bypass grafts. *Journal of Biomechanics, 35*(2), 225–236. doi:10.1016/S0021-9290(01)00194-4

Ngo, N., & Tamma, K. (2001). Microscale permeability predictions of porous fibrous media. *International Journal of Heat and Mass Transfer, 44*(16), 3135–3145. doi:10.1016/S0017-9310(00)00335-5

Onate, E., Celigueta, M., Latorre, S., Casas, G., Rossi, R., & Rojek, J. (2014, May). Lagrangian analysis of multiscale particulate fflow with the particle finite element method. *Computational Particle Mechanics, 1*(1), 85–102. doi:10.1007/s40571-014-0012-9

Pham, Q., Sharma, U., & Mikos, A. (2006). Electrospun poly(E-caprolactone) microfiber and multilayer nanofiber/microfiber scaffolds. Characterization of scaffolds and measurement of cellular infiltration. *Biomacromolecules, 7*(7), 2796–2805. doi:10.1021/bm060680j

Probst, M., Lulfesmann, M., Nicolai, M., Bucker, H., Behr, M., & Bischof, C. (2010). Sensitivity of optimal shapes of artificial grafts with respect to flow parameters. *Computer Methods in Applied Mechanics and Engineering, 199*(17), 997–1005. doi:10.1016/j.cma.2009.11.013

Tura, A. (2003). *Vascular grafts. Experiment and modelling. advances in fluid mechanics* (Vol. 34). Southhampton: WIT Press.

Vafai, K. (2011). *Porous media: Application in biological systems and biotechnology*. Boca Raton, FL: CRC Press, Taylor & F. Group. Retrieved from: https://www.crcpress.com/Porous-Media-Applications-in-Biological-Systems-andBiotechnology/Vafai/p/book/9781420065411#googlePreviewContainer

Vallier, A. (2010). *Tutorial icolagrangianfoam/solidparticle* (Technical Report). Lund Tekniska Hogskola, Lund, Sweden: Peer reviewed tutorial, Hakan Nilsson, CFD with OpenSource Software.

Veit, D. (2012). *Simulation in textile technology. Theory and applications*. Sawston, CA: Woodhead Publishing in association with The Textile Institute. Retrieved from: https://books.google.com.co/books?id=IFwAgAAQBAJ&printsec=frontcover&hl=es#v=onepage&q&f=false

Wang, Y. (2012). *Fabric mechanics*. Retrieved from http://www.fabricmechanics.com

Yang, C., Ding, Y., York, D., & Broeckx, W. (2008). Numerical simulation of sedimentation of microparticles using the discrete particle method. *Particuology, 6*(1), 38–49. doi:10.1016/j.cpart.2007.10.006